International Journal of Mass Spectrometry 285 (2009) 19–25

Contents lists available at ScienceDirect

International Journal of Mass Spectrometry

journal homepage: www.elsevier.com/locate/ijms

Fast and automated large-area imaging MALDI mass spectrometry in microprobe and microscope mode

Leendert A. Klerk, A.F. Maarten Altelaar[1,2], Martin Froesch, Liam A. McDonnell, Ron M.A. Heeren*

FOM Institute for Atomic and Molecular Physics, Kruislaan 407, 1098 SJ, Amsterdam, The Netherlands

ARTICLE INFO

Article history:
Received 23 December 2008
Received in revised form 27 February 2009
Accepted 27 February 2009
Available online 9 May 2009

Keywords:
Microscope imaging mass spectrometry
MALDI
TRIFT

ABSTRACT

Since the introduction of matrix-assisted laser desorption/ionization (MALDI) imaging mass spectrometry (IMS), numerous instrumental developments have been presented. The introduction of microscope MALDI IMS was a major breakthrough, making micron-range resolution MALDI imaging of kiloDalton mass species possible. We discuss new developments that makes large (cm range) field of view, high resolution (μm range) microscope mode imaging mass spectrometry (IMS) possible in a single experiment, using three different data acquisition approaches simultaneously. We demonstrate how a combination of these acquisition approaches is used to correlate mass spectral and high resolution imaging data.

1. Introduction

Since its introduction by Hillenkamp et al. [1,2], the development of matrix-assisted laser desorption/ionization (MALDI) mass spectrometry has made a major impact in many different disciplines, such as plant sciences [3], polymer research [4,5], biomedical sciences, biomaterials engineering [6] and proteomics [7]. The introduction of MALDI imaging mass spectrometry (IMS) opened another range of applications by making it possible to visualize distributions of molecules at surfaces [8,9]. This broad applicability is the driving force behind the numerous instrumental developments, including MALDI mass spectrometers that are customized to imaging mass spectrometry. As a result of these developments, IMS can now be performed on samples that vary in size from a rat whole-body section [10,11] to samples that contain individual cells [12–14].

The most common way of performing an IMS experiment is recording a series of mass spectra at a surface, which is called microprobe mode IMS. In these experiments, a full mass spectrum is stored for a series of *X*–*Y* coordinates, which could otherwise be visualized as an intensity distribution image at each *m*/*z* unit (Fig. 1).

A disadvantage of MALDI IMS is the limited spatial resolution that can be achieved. In a conventional microprobe experiment, the spatial resolution is restricted by the spot-size of the laser. The spatial resolution can be improved by using an oversampling approach [12]. Although the focusing capabilities of modern optics allow submicron laser spot sizes [15], the spot size of the laser should be sufficiently large to obtain good MALDI signal [16], especially when measuring high-mass peptides and proteins. This limits the smallest useful spot size. In addition, the time a measurement takes increases quadratically with a decrease of the spot size.

One unique method to obtain high image resolution in MALDI imaging mass spectrometry is the use of the direct microscope imaging capabilities of the ion optics of the TRIFT (triple focusing time-of-flight) mass spectrometer as was described by Luxembourg et al. [17]. With this method, a large diameter (typically 200 μm) laser beam is used as a desorption and ionization medium. The resulting ion cloud is then transferred by the TOF system in which the ion optics have been designed to retain the original position of the ions orthogonal to the time-of-flight axis as the ions travel through the mass spectrometer (Figs. 2 and 3). An image resolving power of less than 4 μm can be reached by using this methodology. For a MALDI IMS experiment, this implies that the resolving power of an imaging experiment is typically limited by the size of the matrix crystals that are formed with the application of matrix at the sample surface.

The possibility to visualize distributions within the laser spot makes the use of larger laser spots possible and therefore cuts down the measurement time dramatically. The duration of an experiment is determined by the time required for mass analysis (following each laser shot), for transferring each of the mass spectra to memory, the number of laser shots at each position, the time taken to

* Corresponding author. Tel.: +31 20 6081234; fax: +31 20 6684106.
E-mail address: heeren@amolf.nl (R.M.A. Heeren).
[1] Biomolecular Mass Spectrometry and Proteomics Group, Bijvoet Center for Biomolecular Research and Utrecht Institute for Pharmaceutical Sciences, Utrecht University, Sorbonnelaan 16, 3584 CA Utrecht, The Netherlands.
[2] Netherlands Proteomics Centre, Sorbonnelaan 16, 3584 CA Utrecht, The Netherlands.

1387-3806/$ – see front matter © 2009 Published by Elsevier B.V.
doi:10.1016/j.ijms.2009.02.032

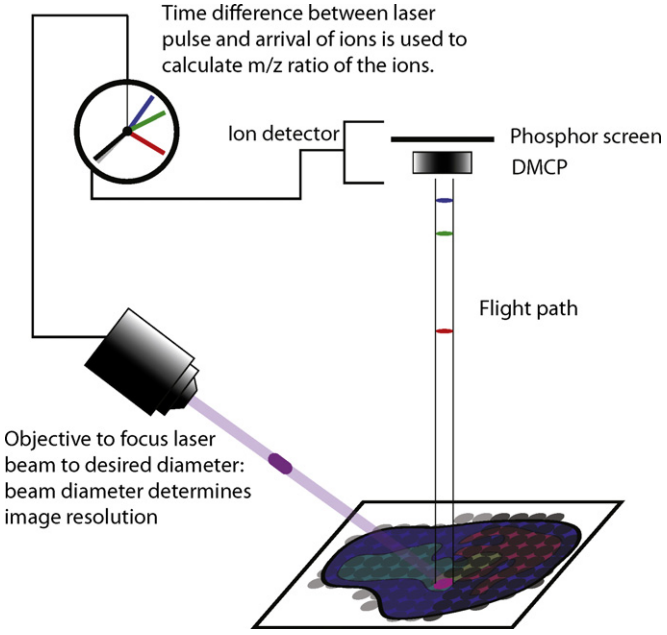

Fig. 1. Schematic overview of a microprobe imaging mass spectrometry setup.

move the sample stage between pixels positions, and the number of sample stage positions in the experiment. The ability to record a 200 μm diameter image with 4 μm resolution with each laser shot using microscope imaging mass spectrometry, means that high resolution images of large samples (composed of a mosaic of high resolution images) can be obtained with a much smaller number of sample stage positions and laser shots than needed for a similar experiment in microprobe mode. Another advantage is that the lower number of laser shots leads to a longer lifetime of the laser. Moreover, the use of a large spot size makes low laser fluence possible, this results in less fragmentation of analytes, higher mass resolution and higher signal/noise ratio [16,18].

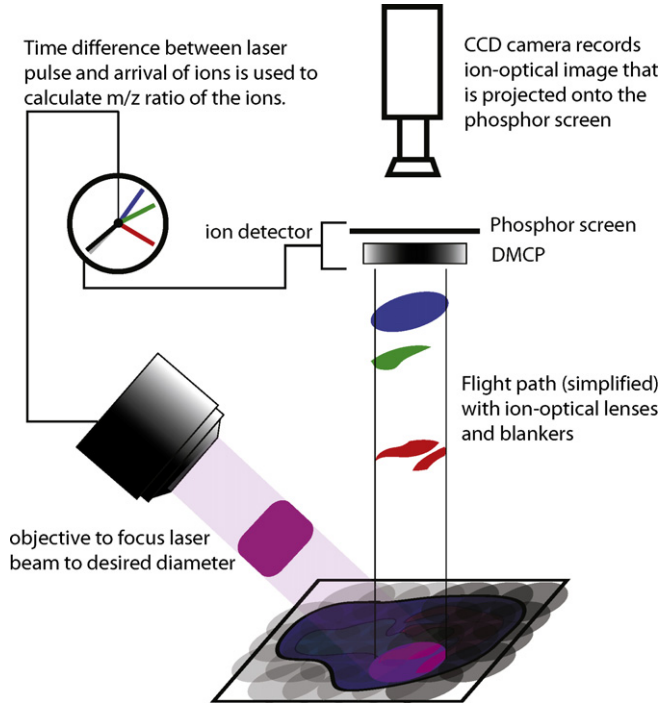

Fig. 2. Schematic overview of a microscope imaging mass spectrometry setup.

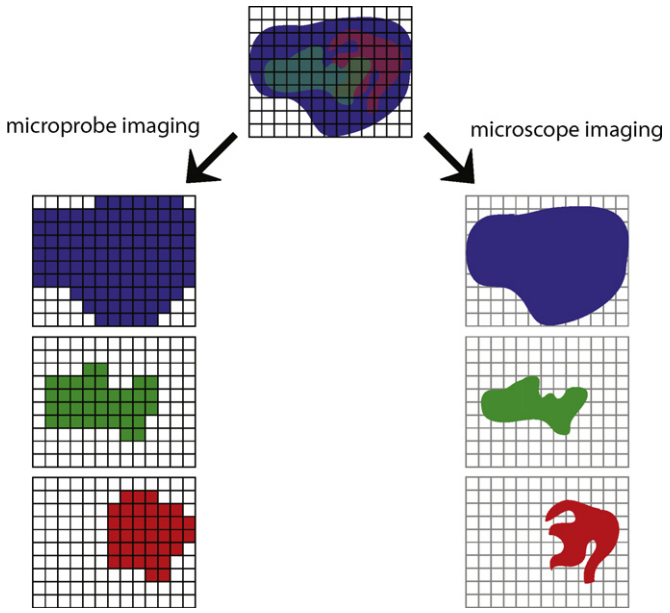

Fig. 3. Comparison of the results of a microprobe (left) and a microscope (right) mode imaging mass spectrometry experiment. The raster in the microscope images is shown as a guide to the eye for means of comparison and has nothing to do with the actual measurement in which a larger distance is used between the different laser shot positions.

Until recently, these microscope-mode MALDI experiments were composed of a combination of multiple semi-continuous linescans [19–21]. Although this method has been proven to give high-resolution images at reasonable measurement time, the linescan methodology is a fairly laborious one because every linescan has to be started manually. Moreover, the number of laser shots that can be added per position is limited to one. Because of the continuous movement of the stage, the position is slightly different for each laser shot. This means that a new dataset (spectrum plus image) is generated for each laser shot. It would be more efficient to add up several datasets that are recorded at the same position. An unsupervised, automated approach that rasters the surface is therefore preferred. This would be similar to imaging as it is performed in most commercial MALDI-TOF microprobe instruments, in which the surface is rastered by moving the stage. Since the introduction of a new version of instrument control software (version 4.3 of WinCadence), rastering of the sample surface is also possible with a TRIFT instrument. In this paper, we show that this offers the opportunity to do fully automated MALDI-TOF microscopy experiments of large sample areas with high spatial resolution. The instrument can acquire microprobe and microscope mode MALDI datasets simultaneously. In this paper we show a new methodology in which both microprobe and high spatial resolution microscope mode imaging are combined. This leads to automated measurements and shorter acquisition times in both microprobe mode and microscope mode imaging.

2. Experimental details

2.1. Instrumentation

The MALDI-MS experiments were performed using a TRIFT II mass spectrometer (Physical Electronics, Eden Prairie, MN). The setup that was used is based on the system that was described previously by Luxembourg et al. [17]. In this paper, we focus on new measurement methodologies that have been implemented since this first MALDI mass microscope was presented. Although we will mention all the fundamentals, we refer to Luxembourg

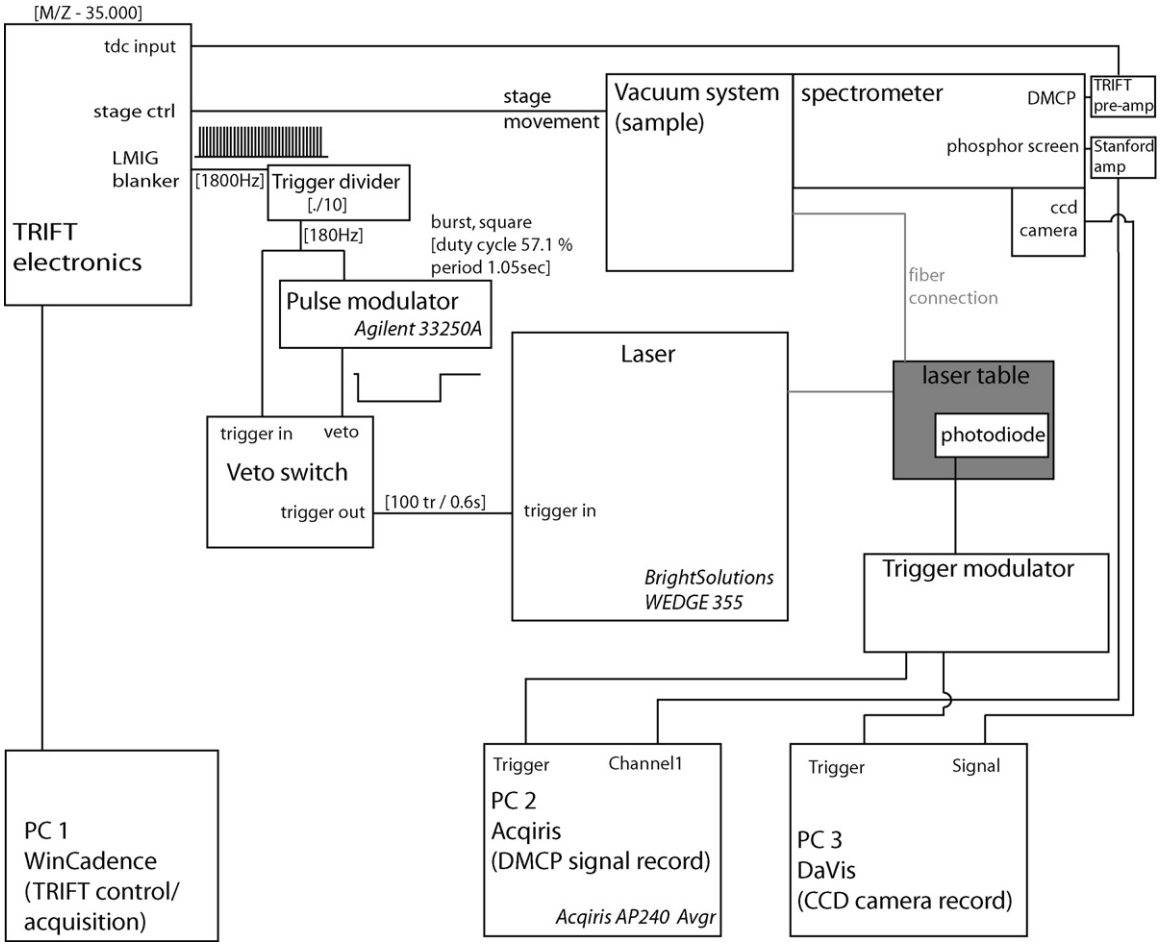

Fig. 4. Schematic of the MALDI TRIFT setup. Timing values are a mere indication and are subject to change according to experimental preference.

et al. [17] for additional technical details as they were described earlier.

A schematic overview of the instrumental setup is given in Fig. 4. All main experimental features are controlled through the TRIFT electronics and WinCadence (Physical Electronics, Eden Prairie, MN) software. Mosaic-mode imaging is used as it is implemented in WinCadence version 4.3 and higher. This allows for automated large-area scans up to 256×256 positions. Each position is measured for typically 0.8 s (although this may be varied upon experimental needs), after which the stage is moved to the next position. The stage movement takes at most 0.3 s. Two different microprobe and one microscope signals can be acquired simultaneously, delivering three intrinsically aligned datasets. These methods are described below.

2.2. Spectral detection system

The detector of the TRIFT has two electronic outputs that are both suited to measure mass spectra: the backside of the dual microchannel plate (DMCP) and the electronic signal from the phosphor screen.

The DMCP signal is connected to the TRIFT's constant fraction discriminator (CFD) and Time to Digital Converter (TDC). This data is recorded through the TRIFT electronics and can be viewed directly in the WinCadende software that is the default acquisition control software for the TRIFT system. This is employed for quick assessment of the data and to tune the various ion blankers. These blankers are used to define an m/z window of ions transmitted in order to measure microscope images of selected ions and to omit ions with a mass outside the mass range of interest. The disadvantage of using the CFD–TDC detection system is that all ions arriving in a certain time window (CFD dead time, typically about 10 ns) are counted as one. This results in a low overall dynamic range for high-intensity signals and is inherent to any ion counting method (Fig. 5). In a secondary ion mass spectrometry (SIMS) [22] experiment this is not an issue due to the low secondary ion count rate combined with the high repetition rate at which is measured. In a MALDI experiment however the number of shots per position is much lower, the ion current much higher and the signal rapidly diminishes due to sample ablation. For MALDI it is common to record the complete output of the detector using an analogue-to-digital-conversion (ADC) system. In this case the

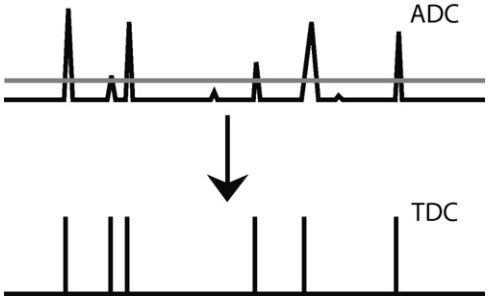

Fig. 5. A comparison between the use of a analog-to-digital convertor (ADC, top) and a time-to-digital converter (TDC, bottom). The use of a TDC system leads to loss in dynamic range and loss of low (below cutoff threshold) signals. The use of a TDC does reduce the data size considerably.

phosphor screen electronic signal output is recorded with a digital oscilloscope computer board (Acqiris DP214 or Acqiris AP240 with Averager). The oscilloscope with averager is the preferred tool to use and constitutes a major improvement compared to the DP214: the direct averaging of all shots per position gives a considerable decrease in total data load, which makes experiments faster and the overall signal-to-noise ratio per position higher.

The analog signal that is recorded from the phosphor screen is proportional to the number of electrons that hit the phosphor screen. Although the number of electrons that are generated in a DMCP setup depends on the DMCP settings, the velocity and nature of the detected ion [23], the number of electrons that hit the phosphor screen is a value that is correlated with the number of ions that hit the DMCP and therefore a good measure for the signal intensity.

To accommodate the relatively high signals from the phosphor screen electronic output, we use an external amplifier (two channels in series of a Stanford Research Systems SR445A four channel DC to 350 MHz amplifier) with an amplification factor of 25 for the recording of the analog signal. This external amplifier tops off the signals that exceed the saturation level. The topping-off of the signal could result in misleading signal strength but is minimized by choosing the proper laser power in order to keep the signal below the clipping threshold as much as possible. The lowest possible laser power would be just above the MALDI threshold, i.e., just high enough to obtain signal from the analyte [24]. Also the DMCP could suffer from saturation due to high ion loads. To reduce both DMCP and amplifier saturation, only the mass range of interest is measured. The TRIFT's blanking system is used to remove the less-interesting, high-velocity and highly abundant low-mass ions.

The measurement of the spectra from the phosphor screen with the ADC computer board is initiated by a trigger pulse that results from a photodiode that picks up stray light of the laser beam. This trigger source is used to minimize any possible jitter in the timing of the laser shot compared to the TRIFT's master trigger, which would lead to poor spectral resolution in case multiple spectra are summed.

2.3. Microscope image recording

To fully benefit from the high spatial resolution imaging capabilities of the TRIFT, even for large samples, a mosaic of microscope mode images can be recorded as the sample is rastered. The principles of ion-optical microscope image recording are explained by Luxembourg et al. [17]. These microscope mode images are recorded from the light output of a phosphor screen detector assembly (APD 30 25 12/10/12 PS I EDR 60:1 P-20 MgO-coated, Burle Industries GmbH, Baesweiler, Germany) using a fast CCD camera with 9.9-μm pixel size (Imager 3, La Vision, Goettingen, Germany). A zoom lens (Thales Optem, Fairport, NY) is used to adjust the phosphor screen image size to fit the CCD chip.

When certain parts of the mass spectrum are selected, and all other ions are blanked, the microscope images give a very high resolution MALDI-TOF MS selected ion image in which spatial biomolecular details can be seen that cannot be resolved otherwise [17]. After acquisition, the microscope images are combined into one overall image using in-house developed software [21].

Total ion current (TIC) microscope images provide a more detailed view on the morphology of the sample. TIC microscope images and microprobe spectral data, that are intrinsically aligned with each other, are combined for a more thorough understanding of the sample, correlating morphological details with mass spectral data [19].

2.4. Laser system

MALDI is performed using the third harmonic of a BrightSolutions WEDGE, diode-pumped solid-state Nd-YAG laser source, at 355 nm wavelength and 5 ns pulse duration (Bright Solutions Soluzioni Laser Innovative srl, Cura Carpignano (PV), Italy). Lower-mode light is filtered out using an optical table with wavelength-specific mirrors. The 355 nm light is then led to the TRIFT system through a fiber optic connection and fed into the vacuum chamber using a telescope-objective outside the vacuum and a high vacuum resistant objective inside the vacuum. The final effective laser spot at the surface has a diameter between 200 and 80 μm and a top-hat shape [17] (dependant on the exact configuration used).

2.5. Materials

α-Cyano-4-hydroxycinnamic acid (HCCA) (>99% by HPLC) and trifluoroacetic acid (TFA) (99.9%) ware obtained from Sigma–Aldrich, Zwijndrecht, The Netherlands and used without further purification. Ethanol and acetonitrile (Analytical grade) were obtained from Biosolve and water was purified using Millipore Q-Gard 1 with Millipak 40 filter.

2.6. Sample preparation

One sample is a part of a whole-body-section of a rat. The cross-section was kindly provided by Markus Stoeckli, Novartis, Basel, Switzerland. It was coated with α-cyano-4-hydroxycinnamic acid (HCCA) using a pneumatic spraying device ('SprayStation' [25]). This gave full matrix coverage in 65 spray-cycles, using a 5 mg/mL HCCA solution in 50% ethanol + 0.1% TFA. After this, the sample was gold coated (5 nm), using a Quorum Technologies SC7640 sputter coater.

Two samples with 5×5 arrays of different peptides or lipids were prepared as a check for microprobe sensitivity and image resolving power.

The peptide mixture contained Bradykinin(1-5) (MW 572.7 Da, 2.0 pmol/μL), Angiotensin II (MW 1046.2 Da, 1.2 pmol/μL), Neurotensin (MW 1672.9 Da, 0.8 pmol/μL) and bovine Insulin chain B (MW 3495.9 Da, 5.0 pmol/μL) in a solution of 5 g/L 2,5-dihydroxybenzoic acid (2,5-DHB) in acetonitrile/water (30:70 v/v) and 0.1% TFA.

The lipid mixture contained cholesterol (MW 386.3 Da) and 1-hexadecanoyl-2-(9Z-octadecenoyl)-sn-glycero-3-phosphocholine 1-palmitic-2-oleic-phosphatidylcholine (PC34:1, MW 760.1 Da) at a concentration of 1 mg/ml in 5 g/L 2,5-DHB in methanol. All commercial samples were purchased from Sigma–Aldrich. The mixtures were spotted on a stainless steel plate using a Shimadzu CHIP-1000 (Shimadzu Corporation, Kyoto, Japan) chemical inkjet printer. Droplet-to-droplet distance was 300 μm for the peptide mix and 400 μm for the lipid mix. The droplets were spotted in multiple cycles, with a total of 20 nL solution per position.

A transverse rat brain section (10 μm thick on indium tin oxide coated glass) was kindly provided by Roger Adan, Utrecht University, The Netherlands. The section was prepared to test combined microprobe and microscope mode imaging. The section was stored at −80 °C and washed directly from −80 °C storage, using 2 washing steps in 70% ice-cold ethanol for 1 min each. After each washing step, the samples were dried under nitrogen flow. Matrix was applied from a solution of 4 mg/mL HCCA in 50% acetonitrile with 0.1% TFA, using a pneumatic spraying device (SprayStation [25]). A 2.5 nm gold layer was deposited for charge compensation [13].

3. Results

3.1. Whole rat section

The whole-rat section was measured exclusively with TDC. The TRIFT's master trigger was used to trigger the laser and the data

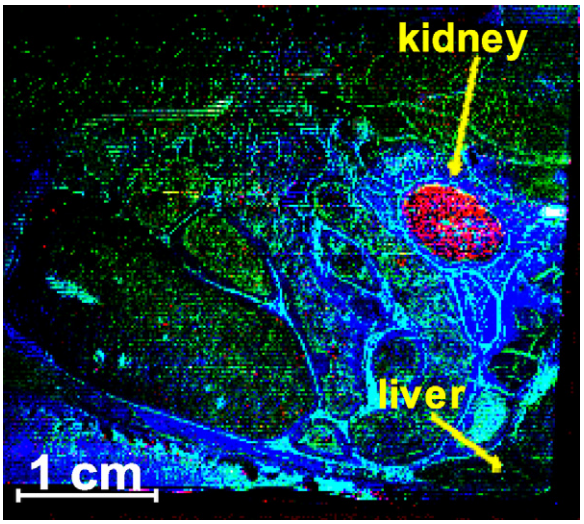

Fig. 6. Part of a whole-rat cross-section (head right, tail left). Various distributions are found in the low-molecular weight region. Blue: free choline (m/z 104), green: phosphocholine (m/z 184), red: a pharmaceutical metabolite (m/z 224). Phosphocholine is localized between the organs, the pharmaceutical metabolite is concentrated in the kidney region. Note the difference in phosphocholine and free choline distribution. This shows how IMS can be used to trace pharmaceutical metabolites after in vivo testing. (For interpretation of the references to colour in this figure legend, the reader is referred to the web version of the article.)

was recorded using the TDC that is default for the TRIFT system as it is in a SIMS configuration. The advantage of this method is that the system is easy to set up, the whole experiment can be controlled from one software package and data analysis is relatively straightforward. Inherent to TDC data acquisition is the resulting relatively small data size. The use of a very high laser rep-rate (1667 Hz), allows for operation at the MALDI threshold (at the risk of some "useless" shots [24]) and it yields sufficient spectral intensity at reasonable measurement time. The overall signal for low-mass compounds is intense enough to resolve localized features. This is shown in Fig. 6. Only the low m/z range was measured. Localization of phosphocholine (m/z 184) between the organs and the pharmaceutical related localization at m/z 224 in the kidney are seen. This method is less useful for the measurement of, typically low-abundant, high-mass ions. However, the high rep-rate laser operation allows for quick imaging of (high-abundant) low-mass molecules like cholesterol, lipid headgroups and pharmaceutical compounds or metabolites. Conclusively, the main reason to do TDC measurements is for quick exploration of the data in order to set the instrumental parameters like the blanking of selected m/z values. ADC data is stored to perform post-acquisition analysis of high-quality data, whereas TDC is used for quick, on-the-fly access.

3.2. Droplet standards

The droplet standards were measured in microprobe mode using a 16×16 sample mosaic with 100 μm step size and 87 summed shots per position at 100 Hz. Analog to digital conversion (ADC) of the phosphor screen signal was done with the Acqiris AP240 with Averager digitizer board. With this number of laser shots per position, TDC acquisition offers a too low dynamic range to be useful for data analysis. The use of a laser spot with a diameter of ~170 μm with a 100 μm step size leads to a small overlap between positions. As signal yield has dramatically decreased after the 87 shots, this does not give a significant overlap effect, but creates a resolving power that is higher than the actual laser spot size [12]. This methodology gives very clear spectral details with a signal/noise of about 175. Despite the relatively low image resolution at which the samples were measured, after bicubic interpolation the images are in good accordance with the crystals that are seen in the optical images (Figs. 7 and 8). This shows that interpolation can be beneficial for the visualization of data. Although this method is commonly used, it should always be noted that the resolution of the experiment is lower than the image suggests. This experiment thus shows that good results can be obtained in microprobe mode using ADC based data acquisition techniques. The spectral data is of high quality and the spatial data is accurate, yet restricted by

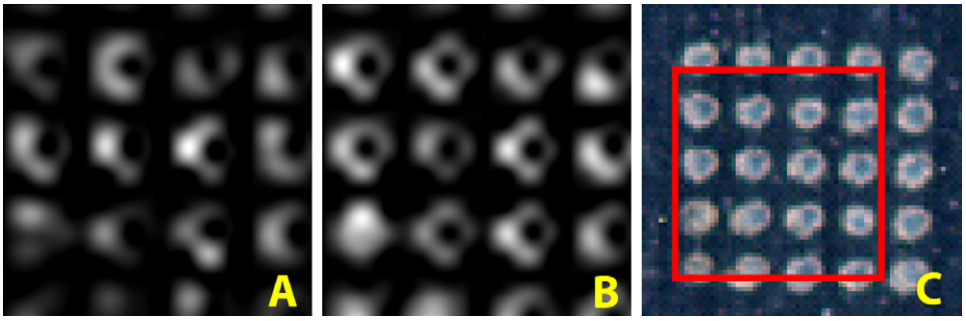

Fig. 7. Microprobe MALDI-TOF images of standards in DHB. Images are from specific peaks: cholesterol (A, m/z 386.3) and phosphatidylcholine (B, m/z 761.8). The samples were measured in a 16×16 mosaic. The localizations after simple interpolation correspond perfectly with the optical (scanned) image (C).

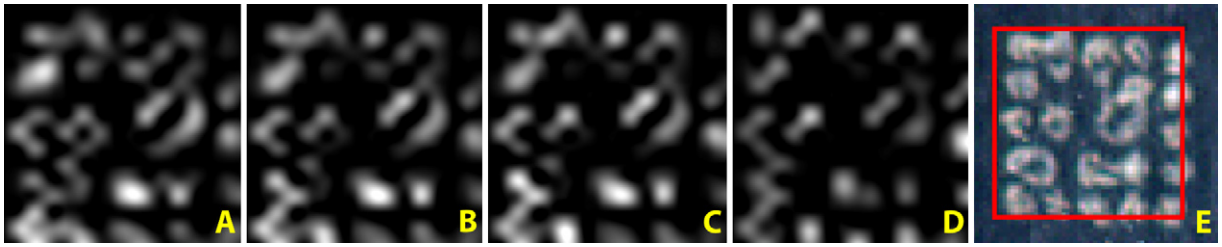

Fig. 8. MALDI-TOF images of standards in DHB are from specific peaks: Bradykinin [1–5] (A, m/z 573.3), angiotensin II (B, m/z 1046.6), neurotensin (C, m/z 1673.0), bovine insulin chain B (D, m/z 3497.1), The MSI images were measured in a 16×16 mosaic. The localizations after simple interpolation correspond very well with the optical (scanned) image (E).

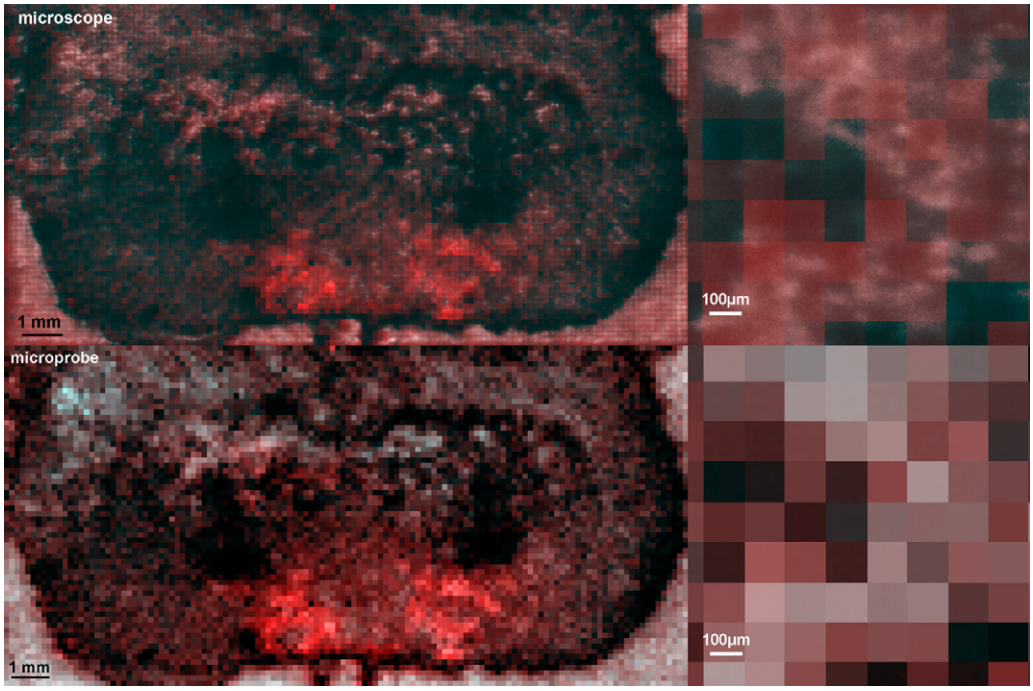

Fig. 9. Microscope and microprobe total ion images with a selected ion image (m/z = 1120 Da) overlay in red. The right images show part of the sample at full resolution. The microprobe selected ion image is naturally aligned with, and can be correlated with microscopic structures in the microscope total ion image. (For interpretation of the references to colour in this figure legend, the reader is referred to the web version of the article.)

the acquisition spot-to-spot distance. This offers the possibility to combine microscope and microprobe IMS in a single acquisition, as shown below.

3.3. Rat brain sample: microprobe and microscope IMS

A transverse rat brain section was measured in a combined microscope and microprobe mode experiment. The Acqiris DP214 board was used for the mass spectral detection. Microscope mode total ion images were recorded from the phosphor screen, using a CCD camera.

The whole brain sample was measured in 8 squares of each 32×32 positions. At each position, 9 spectra and 9 microscope total ion images were recorded and summed. The number of measured spectra at each position and the number of positions per experiment could not be further increased due to memory limitations of the data acquisition card. After acquisition, the spectra were summed to give one single spectrum per position and each position was inserted into one large microprobe hyperspectral datacube using in-house developed software. Additionally, the microscope mode total ion images were summed and one total ion image was constructed using custom-made software [21]. An overlay of a selected ion microprobe image (m/z = 1124 Da) is made with both microscope and microprobe total ion images (Fig. 9). It shows the advantage of the microscope imaging when it comes down to structural details in the image. Structural details in the microscope total ion image can be correlated with a microprobe selected ion intensity map.

4. Conclusions

The TRIFT instrument is demonstrated to be capable of doing µm-resolution microscope mode MALDI-TOF experiments of large areas in an automated way. In which the measured area could range up to several centimeters.

We also demonstrated that the TRIFT instrument is capable of doing large-area MALDI-TOF experiments at high (>1000 Hz) laser repetition rates. Three different acquisition modes each have their own advantages. The microscope images give a high-spatial resolution image. The signal that is recorded with an ADC gives the corresponding mass spectrum. And the data that is recorded with the TRIFT electronics, using a TDC, can be directly viewed in WinCadence during the acquisition and be used for quick access to tune blankers as well as other system parameters.

A TDC acquisition system was also shown to be useful for low-mass MALDI experiments at high laser rep-rate. For MALDI experiments of lower concentration compounds and compounds with higher mass, the use of an ADC as means of detection is clearly preferred. When using an ADC, the peak intensity is best preserved and therefore the high ion loads that are typical for MALDI-MS can be fully used for analysis. Because of limitations inherent to ion counting techniques, this is not possible with a TDC. We showed that an ADC with averaging capabilities is necessary for high-speed large area acquisitions as it gives a large reduction in both data writing time and data file size.

The possibility to combine microprobe and microscope mode imaging offers possibilities to recognize spatial details that cannot otherwise be resolved.

Acknowledgements

This work is part of the research program of the “Stichting voor Fundamenteel Onderzoek der Materie (FOM)”, which is financially supported by the “Nederlandse organisatie voor Wetenschappelijk Onderzoek (NWO). We acknowledge funding from the Strategic Research Fund (SRF) of ICI plc. Part of this work is part of the Computis Program, 6th European Framework Program for Research and Technological Development (FP6), project no. LSHG-CT-2005-5181194. Ivo Klinkert is gratefully acknowledged for the development of data processing tools.

References

[1] F. Hillenkamp, M. Karas, R.C. Beavis, B.T. Chait, Matrix-assisted laser desorption ionization mass-spectrometry of biopolymers, Analytical Chemistry 63 (1991) A1193.

[2] M. Karas, D. Bachmann, U. Bahr, F. Hillenkamp, Matrix-assisted ultraviolet laser desorption of non-volatile compounds, International Journal of Mass Spectrometry 78 (1987) 53.

[3] B. Stahl, A. Linos, M. Karas, F. Hillenkamp, M. Steup, Analysis of fructans from higher plants by matrix-assisted laser desorption/ionization mass spectrometry, Analytical Biochemistry 246 (1997) 195.

[4] G. Montaudo, F. Samperi, M.S. Montaudo, Characterization of synthetic polymers by MALDI-MS, Progress in Polymer Science 31 (2006) 277.

[5] C.G. Dekoster, M.C. Duursma, G.J. Vanrooij, R.M.A. Heeren, J.J. Boon, Endgroup analysis of polyethylene-glycol polymers by matrix-assisted laser-desorption ionization Fourier-transform ion-cyclotron resonance mass-spectrometry, Rapid Communications in Mass Spectrometry 9 (1995) 957.

[6] H.J. Griesser, P. Kingshott, S.L. McArthur, K.M. McLean, G.R. Kinsel, R.B.R.B. Timmons, Surface-MALDI mass spectrometry in biomaterials research, Biomaterials 25 (2004) 4861.

[7] L.R.B. Jasminka Godovac-Zimmermann, Perspectives for mass spectrometry and functional proteomics, Mass Spectrometry Reviews 20 (2001) 1.

[8] L.A. McDonnell, R.M.A. Heeren, Imaging mass spectrometry, Mass Spectrometry Reviews 26 (2007) 606.

[9] D.S. Cornett, M.L. Reyzer, P. Chaurand, R.M. Caprioli, MALDI imaging mass spectrometry: molecular snapshots of biochemical systems, Nature Methods 4 (2007) 828.

[10] M. Stoeckli, D. Staab, A. Schweitzer, Compound and metabolite distribution measured by MALDI mass spectrometric imaging in whole-body tissue sections, International Journal of Mass Spectrometry Imaging Mass Spectrometry Special Issue 260 (2007) 195.

[11] S. Khatib-Shahidi, M. Andersson, J.L. Herman, T.A. Gillespie, R.M. Caprioli, Direct molecular analysis of whole-body animal tissue sections by imaging MALDI mass spectrometry, Analytical Chemistry 78 (2006) 6448.

[12] J.C. Jurchen, S.S. Rubakhin, J.V. Sweedler, MALDI-MS imaging of features smaller than the size of the laser beam, Journal of the American Society for Mass Spectrometry 16 (2005) 1654.

[13] A.F. Altelaar, S.L. Luxembourg, L.A. McDonnell, S.R. Piersma, R.M. Heeren, Imaging mass spectrometry at cellular length scales, Natural Protocol 2 (2007) 1185.

[14] L.A. McDonnell, S.R. Piersma, A.F.M. Altelaar, T.H. Mize, S.L. Luxembourg, P.D.E.M. Verhaert, J. van Minnen, R.M.A. Heeren, Subcellular imaging mass spectrometry of brain tissue, Journal of Mass Spectrometry 40 (2005) 160.

[15] B. Spengler, M. Hubert, Scanning microprobe matrix-assisted laser desorption ionization (SMALDI) mass spectrometry: instrumentation for sub-micrometer resolved LDI and MALDI surface analysis, Journal of the American Society for Mass Spectrometry 13 (2002) 735.

[16] K. Dreisewerd, M. Schurenberg, M. Karas, F. Hillenkamp, Influence of the laser intensity and spot size on the desorption of molecules and ions in matrix-assisted laser-desorption ionization with a uniform beam profile, International Journal of Mass Spectrometer 141 (1995) 127.

[17] S.L. Luxembourg, T.H. Mize, L.A. McDonnell, R.M.A. Heeren, High-spatial resolution mass spectrometric imaging of peptide and protein distributions on a surface, Analytical Chemistry 76 (2004) 5339.

[18] A. Ingendoh, M. Karas, F. Killenkamp, U. Giessmann, Factors affecting the resolution in matrix-assisted laser-desorption ionization mass-spectrometry, International Journal of Mass Spectrometry 131 (1994) 345.

[19] A.F.M. Altelaar, I.M. Taban, L.A. McDonnell, P.D.E.M. Verhaert, R.P.J. de Lange, R.A.H. Adan, W.J. Mooi, R.M.A. Heeren, S.R. Piersma, High-resolution MALDI imaging mass spectrometry allows localization of peptide distributions at cellular length scales in pituitary tissue sections, International Journal of Mass Spectrometry 260 (2007) 203.

[20] A.F.M. Altelaar, I. Klinkert, K. Jalink, R.P.J. de Lange, R.A.H. Adan, R.M.A. Heeren, S.R. Piersma, Gold-enhanced biomolecular surface imaging of cells and tissue by SIMS and MALDI mass spectrometry, Analytical Chemistry 78 (2006) 734.

[21] I. Klinkert, L.A. McDonnell, S.L. Luxembourg, A.F.M. Altelaar, E.R. Amstalden, S.R. Piersma, R.M.A. Heeren, Tools and strategies for visualization of large image data sets in high-resolution imaging mass spectrometry, Review of Scientific Instruments 78 (2007) 053716.

[22] J.C.B. Vickerman, David, ToF-SIMS: Surface Analysis by Mass Spectrometry, IM Publications and SurfaceSpectra Ltd., 2001.

[23] R. Meier, P. Eberhardt, Velocity and ion species dependence of the gain of microchannel plates, International Journal of Mass Spectrometry 123 (1993) 19.

[24] Y.M.W. Ens, F. Mayer, K.G. Standing, Properties of matrix-assisted laser desorption. Measurements with a time-to-digital converter, Rapid Communications in Mass Spectrometry 5 (1991) 117.

[25] M. Stoeckli, D. Staab, S. Capretta, Automated Matrix Deposition for MALDI MSI, 54th ASMS Conference on Mass Spectrometry and Allied Topics, Seattle, WA, 2006.